Monthly Notices
of the
ROYAL ASTRONOMICAL SOCIETY

MNRAS **476,** 999–1009 (2018) doi:10.1093/mnras/sty209

Towards an automatic wind speed and direction profiler for Wide Field adaptive optics systems

G. Sivo,[1★] A. Turchi,[2] E. Masciadri,[2★] A. Guesalaga[3] and B. Neichel[4]

[1]*Gemini Observatory, AURA, Colina el Pino s/n, Casila 603, La Serena, Chile*
[2]*INAF Osservatorio Astrofisico di Arcetri, Largo Enrico Fermi 5, I-50125 Florence, Italy*
[3]*Pontificia Universidad Catolica de Chile, 4860 Vicuna Mackenna, Casilla 7820436, Santiago, Chile*
[4]*Aix Marseille Université, CNRS, LAM Laboratoire d'Astrophysique de Marseille UMR 7326, F-13388 Marseille, France*

Accepted 2018 January 20. Received 2017 December 20; in original form 2017 September 26

ABSTRACT

Wide Field Adaptive Optics (WFAO) systems are among the most sophisticated adaptive optics (AO) systems available today on large telescopes. Knowledge of the vertical spatio-temporal distribution of wind speed (WS) and direction (WD) is fundamental to optimize the performance of such systems. Previous studies already proved that the Gemini Multi-Conjugated AO system (GeMS) is able to retrieve measurements of the WS and WD stratification using the SLOpe Detection And Ranging (SLODAR) technique and to store measurements in the telemetry data. In order to assess the reliability of these estimates and of the SLODAR technique applied to such complex AO systems, in this study we compared WS and WD values retrieved from GeMS with those obtained with the atmospheric model Meso-NH on a rich statistical sample of nights. It has previously been proved that the latter technique provided excellent agreement with a large sample of radiosoundings, both in statistical terms and on individual flights. It can be considered, therefore, as an independent reference. The excellent agreement between GeMS measurements and the model that we find in this study proves the robustness of the SLODAR approach. To bypass the complex procedures necessary to achieve automatic measurements of the wind with GeMS, we propose a simple automatic method to monitor nightly WS and WD using Meso-NH model estimates. Such a method can be applied to whatever present or new-generation facilities are supported by WFAO systems. The interest of this study is, therefore, well beyond the optimization of GeMS performance.

Key words: turbulence – atmospheric effects – balloons – methods: data analysis – methods: numerical – site testing.

1 INTRODUCTION

Wide Field Adaptive Optics (WFAO) systems are among the most technologically advanced and complex AO systems installed or to be installed on large telescopes. The term WFAO includes a few types of adaptive optics: laser tomography adaptive optics (LTAO), multi-conjugated adaptive optics (MCAO), ground-layer adaptive optics (GLAO) and multi-object adaptive optics (MOAO). All WFAO systems have the common characteristics of significantly increasing the field of view (FoV) of images obtained after AO correction and the portion of sky that becomes accessible after reconstruction of the original wavefront. Indeed, WFAO can obtain a corrected wavefront on a field of view of the order of a few arcmin. This is larger than the few arcseconds, typical of single-conjugated adaptive optics (SCAO) systems. In WFAO systems, light from a set of guide stars (GSs) located in dedicated configurations on the sky is used to probe the instantaneous 3D phase perturbations and an inverse problem procedure is used to reconstruct the turbulence in the sensed volume. This technique is known as atmospheric tomography. Tallon & Foy (1990) proposed this technique for the first time and later some improvements were suggested by several other authors (Johnston & Welsh 1994; Ellerbroek 1994; Fusco et al. 2001).

Knowledge of the three-dimensional turbulence distribution, as well as the wind speed (WS) and wind direction (WD) stratification for the whole atmosphere, strongly affects the performance of all WFAO systems. Tomographic performance can be significantly deteriorated by the wrong quantification of the atmospheric state (Neichel, Fusco & Conan 2008). The geometry of the system is strictly correlated with some important limitations (among others, the modes and turbulence not seen by the system). The regularization of these modes is affected by errors in identification of the height of the recovered turbulent layers. The sensitivity of the reconstructors to unseen frequencies is related strictly to the height of the recovered layers seen by the AO system. A wrong geometry

★ E-mail: gsivo@gemini.edu (GS); masciadri@arcetri.astro.it (EM)

implies that the regularization acts in an inefficient way. Different articles report analyses on how errors of the model affect the turbulence quantification. Conan et al. (2001) and Tokovinin & Viard (2001) investigated how the reconstructed error is influenced by an error in the estimate of the C_N^2 profile; Le Louarn & Tallon (2002) studied the relationship between the reconstruction of a limited number of turbulent layers at discrete altitudes and the whole volume of atmospheric turbulence; Fusco et al. (1999) explored the impact on the reconstruction of the wavefront caused by employing a small number of equivalent layers. Conclusions indicated that a small number of layers (2–3) was sufficient to reconstruct a uniform corrected field; more recently, however, Costille & Fusco (2012) concluded that, for an application to Extreemely Large Telescopes (ELTs), the sampling of the C_N^2 profiles (i.e. the ability to reconstruct thin turbulence layers) plays an important role in the performance of the system and the number of turbulent layers necessary for reconstruction of the wavefront can be higher than this. All the above previous investigations tell us that the FoV is directly proportional to the sensitivity of the AO system with respect to errors caused while identifying the height and position of the layers. Besides the C_N^2 profiles, a good WS and WD estimate is required for efficient employment of an MCAO system: first because the WS, together with the C_N^2, determines the value of the wavefront coherence time (τ_0) that tells us how fast an AO system has to run and secondly because errors in time in AO are produced by modification of the turbulence between the instant at which a perturbed wavefront is sensed and the instant at which it is corrected. This is known as a 'control cycle'. If the turbulence is assumed to be frozen, the forecast of the state of a turbulent layer at a time in the future depends on the state of the WS and WD of the atmospheric turbulent layer at present (Johnson et al. 2008). By using the CANARY demonstrator at the William Hershel Telescope, it has been demonstrated, on-sky, that a predictive control, based on a linear quadratic Gaussian (LQG) controller fed by atmospheric turbulence priors such as C_N^2 and wind speed profiles (only wind speed during that experience), improved the system performance significantly with respect to a classic integral controller. It is shown that, in classical AO, the improvement in the Strehl ratio is of the order of 10 per cent in the K band on average (Sivo et al. 2014). This predictive control has also been validated in WFAO (MOAO configuration). It has also been shown that, by using LQG control, better performance is obtained than by using a standard minimum mean-squared error (MMSE) reconstructor. The gain in performance is clear when the wind speed profile, given *'a priori'* to the model, is close to the real one (Sivo et al. 2013; Osborn et al. 2015). Recently, Ono et al. (2016) also dealt with the advantages one can obtain in knowing the wind speed in applications to wavefront reconstruction in MOAO systems conceived for ELTs. Knowing the WS and WD of the different turbulent layers is, therefore, very important to reconstruct the state of the phase in the time-scale of the control cycle, as other authors stated (Gavel & Wiberg 2002; Poyneer, MacIntosh & Veran 2007; Ammons et al. 2012). The last article also treated as evidence the potential additional benefit to tomographic AO systems in knowing the WS: the combination of wind speed and phase height information from multiple guide stars breaks inherent degeneracies in volumetric tomographic reconstruction, producing a reduction in the geometric tomographic error.

In this article, we perform a comparison between wind speed reconstructed by the mesoscale non-hydrostatic atmospheric model Meso-NH and that measured by GeMS for a sample of 43 nights, very representative from a statistical point of view. Previous studies (Masciadri, Lascaux & Fini 2013, 2015) proved that the Meso-NH model could reconstruct reliable WS and WD profiles for the total atmosphere (from 0–20 km above the ground) above one of the best astronomical sites in the world (Cerro Paranal in Chile). A comparison of model predictions with 50 radiosoundings launched in winter and summer of the same year has been studied in statistical terms. For the wind speed, a bias has been found within 1 m s^{-1} and a root-mean-square error (RMSE) within 3 m s^{-1} in the range 5–15 km. In the 3–5 km range and above 15 km, the bias is within 2 m s^{-1}. Also, a dedicated study performed on all 50 couples (radiosoundings and model profiles: Masciadri et al. 2013, fig. B1) told us that a similarly satisfactory performance was obtained by the model in statistical terms and also by comparing radiosoundings versus model ouputs for each individual couple. It is possible to conclude, therefore, that the Meso-NH model could be taken as a reference to validate the WS and WD provided by GeMS. The distance between Cerro Paranal and Cerro Pachón is indeed of the order of 600–700 km and they are located in the same Chilean mountain region. There is, therefore, no reason to assume that the model can provide different reliability in its estimates for the two sites for vertical stratification of WS over the whole 20 km.

The goal of this article is to validate the reliability of GeMS estimates as a profiler of WS and WD and, equally, to investigate whether it possible to use Meso-NH to feed GeMS to obtain an efficient automatic WS and WD profiler applied to WFAO systems. Indeed, as will be described later on, the procedure to automate GeMS measurements is particularly complex and it appears more suitable to use WS and WD estimates from the Meso-NH model, which offers the advantage of being a technique more complete in time (a temporal frequency of two minutes during the whole night versus a limited number of detections as obtained by GeMS, as will be described later on). The Meso-NH model also offers better spatial coverage, i.e. 62 vertical levels instead of the typical 2–3 layers detected by GeMS. Besides this, it is important to remind the reader that the important information for a WFAO system is the detection of the wind speed where there are turbulent layers. It is worth stating that it has been observed that rapid changes of atmospheric conditions, including WS and WD, determine the negative effects on the quality of observations taken with GeMS. In the operational phase, it is extremely useful to know the state of the WS and WD as measured by GeMS. It would even be preferable to know the wind speed in advance with the Meso-NH model. If one knows the WS and WD in advance, this information might be used, for example, to update the control matrices with an increment or reduction of the relative gains related to the height of each turbulent layer if it is joint to knowledge of C_N^2. Knowing the WS and WD is extremely useful in the context of predictive control, for example for tip–tilt control (Sivo et al. 2014; Juvenal et al. 2016).

2 OBSERVATIONS

GeMS, the MCAO facility installed at Gemini South, is currently the first laser guide star (LGS)-based MCAO system using sodium stars in regular operation dedicated for astronomical observations (Neichel et al. 2014a; Rigaut et al. 2014). It employs five LGSs projected on a 1-arcmin^2 asterism (four at the corners and one in the middle). GeMS uses this artificial asterism to measure and correct for atmospheric perturbations and provides an almost diffraction-limit-corrected image in the near-infrared (NIR) over a wide FoV of about 2 arcmin. GeMS is currently feeding three scientific instruments: a 4 k × 4 k NIR imager called Gemini South Adative Optics Imager (GSAOI) (McGregor et al. 2004), a wide FoV NIR imager and spectrograph Flamingos2 (Elston et al. 2003) and more

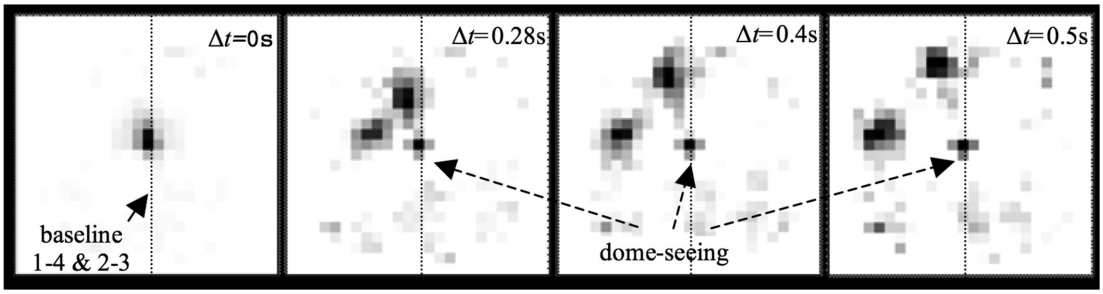

Figure 1. The sequence reported in the figure shows the correlation time from $\Delta t = 0$ to $\Delta t = 0.5$ s, with two layers moving in different directions. In the centre of each individual square a third static peak is visible, corresponding to the dome seeing.

recently a visible multi-object spectrograph and imager Gemini Multi Object Spectrograph-South (GMOS-S) (Crampton et al. 2000; Hibon et al. 2014, 2016).

We retrieve turbulence and WS profiles by employing a procedure presented in Cortes et al. (2012) that uses the SLOpe Detection And Ranging (SLODAR) technique applied to binaries (Wilson 2002) and adapted to multiple LGSs available on WFAO instruments working with Shack–Hartmann wavefront sensors (Gilles & Ellerbroek 2010; Cortes et al. 2012; Osborn et al. 2012). Turbulence strength has been sampled with a vertical resolution equal to $\Delta h = d/\theta$, where d is the sub-aperture of the wavefront sensor projected on the pupil and θ the angular distance of different couples of stars chosen from among the LGS constellation of GeMS. Depending on the selected binaries, we can therefore obtain different Δh. Since we use LGSs, we need to deal with a well-known limitation called the *cone effect*. This implies that bins along the z-axis have a different size (see equation 1 in Cortes et al. 2012).

As an extended version of the SLODAR technique, we determine the wind vertical *profiling* by computing cross-correlations with different delay times between all different vectors of arrival angles, i.e. slope measurements from the valid WFS sub-apertures (Wang, Schoek & Chanan 2008). This profiling technique provides information on how the turbulence is distributed in the atmosphere and the temporal evolution of the WS and WD of all identified layers. In the case of GeMS, since LGSs are centre-launched, the slopes suffer from the fratricide effect. The method has also been modified to tackle this issue (Guesalaga et al. 2014).

The selection of observations has been done manually in this analysis. That means that GeMS measurements have been selected in such a way that cross-correlation peaks (related to turbulent layers moving rigidly in the atmosphere) are clearly detected without ambiguity. To detect the WS of a layer, it is required to follow the displacement of the peak in the cross-correlation map. These peaks are more easily recognized when the atmosphere is characterized by turbulent layers placed at different heights with different velocities, which produce peaks with relative tracks that do not overlap. Data analysis is performed following the procedures developed in Cortes et al. (2012) and Guesalaga et al. (2014). For each telemetry file, a cross-correlation temporal movie is built. Fig. 1 shows a sequence of images selected from one of the temporal movies. The WS is retrieved from the displacement of the correlation peak over a given Δt. For the WS uncertainties we assumed a ± 0.2 to ± 0.5 sub-aperture error, depending on the signal-to-noise ratio of the peak, and ± 1 to ± 2 frame error, depending on the shift velocity of the peak. Uncertainties in the estimation of heights are based on the size of the altitude bin, as reported in Cortes et al. (2012). As reported in Section 4.1, the uncertainty along the z-axis is of the order of $\pm[0.5, 0.8]$ km.

3 MODEL

We performed numerical simulations on the selected 43-night sample using Meso-NH (Lafore et al. 1998), which is a non-hydrostatic mesoscale atmospheric model developed by the Centre National des Recherches Météorologiques (CNRM) and the Laboratoire d'Aéreologie (LA) of Université Paul Sabatier (Toulouse). Like all mesoscale models, Meso-NH provides spatio-temporal evolution of meteorologic parameters on a 3D spatial scale, over a finite region of the Earth. The anelastic formulation of the set of hydrodynamic equations allows for the filtering of acoustic waves. The physical exchange between soil and atmosphere is computed by making use of the Interaction Soil Biosphere Atmosphere (ISBA) module (Noilhan & Planton 1989). The model uses the Gal-Chen & Sommerville (1975) coordinate system on the z-axis and the C-grid (in the formulation of Arakawa & Messinger 1976) for the spatial digitalization. The time evolution scheme uses a custom three-step time-filtered leapfrog, as described in Asselin (1972). The turbulence model is a one-dimensional 1.5 turbulence closure scheme (Cuxart, Bougeault & Redelsperger 2000), with a one-dimensional mixing length first described by Bougeault & Lacarrère (1989). From the basic turbulence scheme, the optical turbulence parameters (C_N^2 and derived integrated parameters) are computed with the Astro-Meso-NH package developed by Masciadri, Vernin & Bougeault (1999). The last package has seen a great amount of development in recent years, supporting many studies that addressed the reliability of this forecast method in astronomical applications (Masciadri, Avila & Sanchez 2004; Masciadri & Egner 2006; Hagelin et al. 2011; Lascaux, Masciadri & Hagelin 2011). A few among these studies have been directly focused on the ability of Meso-Nh in reconstructing wind speed (Masciadri & Garfias 2001; Hagelin et al. 2010; Masciadri et al. 2013). The most recent version of the Astro-Meso-NH code has been described in Masciadri, Lascaux & Fini (2017). The Meso-NH and Astro-Meso-NH models have been parallelized with OPEN-MPI with a great degree of scalability, allowing users to make use of multi-core workstations, local clusters or even large high-performance computing facilities (HPCF), in our case the HPC of the European Centre for Medium-Range Weather Forecasts (ECMWF), and achieving, under specific model configurations, a smaller computing time.

Simulations have been performed above the site of GeMS, i.e. Cerro Pachón at (70°44′12.096″W; 30°14′26.700″S).[1]

To maximize the resolution of the simulations over the site of interest, we used the so-called 'grid-nesting' technique, which consists of producing multiple (three in this case) imbricated model

[1] http://www.gemini.edu/sciops/telescopes-and-sites/locations

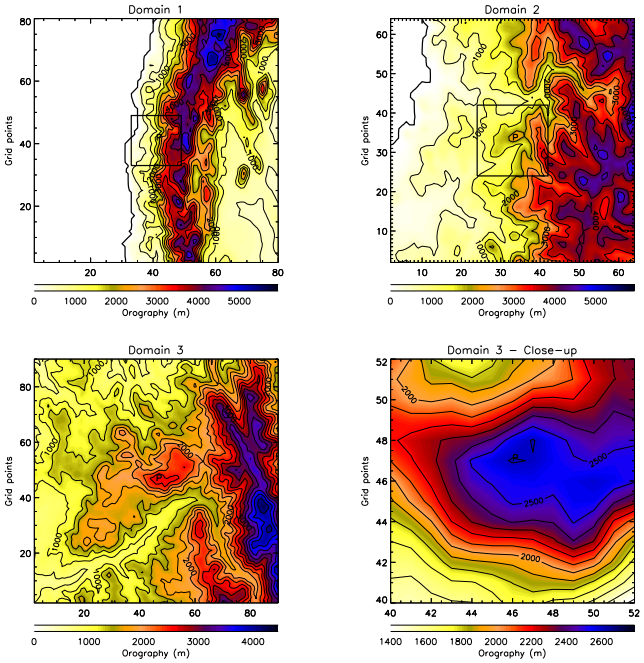

Figure 2. Topography. Domain 1 (top left): 80 × 80 grid points, 100 × 100 km for $\Delta(X) = 10$ km. Domain 2 (top right): 64 × 64 grid points, 160 × 160 km for $\Delta(X) = 2.5$ km. Domain 3 (bottom left): 90 × 90 grid points, 45 × 45 km for $\Delta(X) = 0.5$ km. A zoom of the summit extracted from Domain 3 is shown on the bottom right.

Table 1. Grid-nesting configuration of the Meso-NH model. The number of horizontal grid points is reported in the second column, the domain extension for each imbricated domain in the third column and the horizontal resolution ΔX in the fourth column.

Domain	Grid points	Domain size (km)	ΔX (km)
Domain 1	80 × 80	800 × 800	$\Delta X = 10$
Domain 2	64 × 64	160 × 160	$\Delta X = 2.5$
Domain 3	90 × 90	45 × 45	$\Delta X = 0.5$

domains, each progressively extended on smaller surfaces and at increased horizontal resolution and centred on the Cerro Pachón coordinates, up to a maximum resolution of the innermost domain $\Delta X = 500$ m (see Fig. 2 and Table 1). The vertical grid remains identical in each domain. It has already been proven in a previous study (Masciadri et al. 2013) that this model configuration, together with the detailed 500-m resolution of the innermost domain, allows one to obtain excellent results in terms of the vertical stratification of wind speed and direction, which are the parameters of interest in this study. The digital elevation model (DEM, i.e. topography) used for the most external domains (1 and 2) is GTOPO30,[2] which has an intrinsic horizontal resolution of 1 km. In domain 3, we used the Shuttle Radar Topography Mission (SRTM)[3] topography, which has an intrinsic horizontal resolution of 90 m. The model interpolates the innermost DEM using the specific horizontal resolution of 500 m, as reported in Table 1. In Fig. 2, we show a graphical representation of the three imbricated domains.

We used a vertical grid of 62 levels, which covers the whole atmosphere up to ∼20 km above ground level (a.g.l.), starting from an initial point at 5 m a.g.l., with a progressive logarithmic stretching of 20 per cent up to 3.5 km a.g.l. From this last height onward, the model uses an almost constant grid size of 600 m. Even if the number of model levels can be freely chosen and is not a constraint for the model, it is in our interest to limit the number of vertical model levels to what it is necessary to avoid increasing the computation time. We note that there are no turbulent layers (i.e. no WS measurements) detected by GeMS at heights higher than 18 km a.s.l. The configuration chosen is therefore suitable for this study. Besides that, we highlight that this configuration is also suitable to estimate τ_0 (Masciadri et al. 2017). Indeed, if we look at the climatology of C_N^2 at latitudes typical of astronomical observatories, we observe that the optical turbulence is very weak above 20 km (for example Garcia-Lorenzo & Fuensalida 2011a,b). If we look at the climatology of the WS, we observe that the wind speed reaches a maximum at 11–13 km and then decreases inexorably at heights of the order of 20 km or more (see for example Hagelin, Masciadri & Lascaux 2010). This is therefore a reasonable spatial scale.

We performed numerical simulations on a total of 43 nights for which we have GeMS telemetry data available. For each night, identified by the UT date, the simulation was initialized at 1800 UT on the previous day and new updated *forcing* data was fed to the simulation every 6 h, using analysis input data produced meanwhile by the Global Circulation Model of ECMWF. Each simulation lasted up to 1100 UT (0700 LT), for a total simulation length of 17 h. The temporal sampling of the model outputs, i.e. vertical wind profiles, is 2 min; however, the analysis performed in this article made use only of the specific data referring to local night times for those selected times during which observations/measurements are available.

4 RESULTS

4.1 Wind speed

To guarantee a fair analysis, the data reduction of GeMS measurements and Meso-NH simulations related to the whole sample of 43 nights has been performed in a totally independent way. To have an idea of the features of the WS reconstructed by the model, Fig. 3 reports the temporal evolution of the WS vertical profiles during the whole night for a subsample of nights. The black vertical lines correspond to the time during which we have WS measurements from GeMS. At each instant, GeMS detects WS measurements associated with a finite number of layers (typically one to three layers). By this, we mean that the maximum number of layers retrieved from the technique we have described is not more than around three layers. This does not mean that in the atmosphere there are just three layers, but that the method is able to discern three layers. This is due to the vertical resolution of the system, but also a set of reasons that will be described in Section 5. Looking at Fig. 3, it appears evident that, for each night, the number of estimates from GeMS is smaller than the available estimates from the model, but in this context we are interested in the evaluation of the method performed by GeMS; therefore this element is not critical. The important thing is to have a rich statistic of couples [observations, model outputs] to be treated.

We compared model outputs with measurements for the statistical sample of 43 nights, which corresponds to around 400 couples of

[2] https://lta.cr.usgs.gov/GTOPO30
[3] http://srtm.csi.cgiar.org/

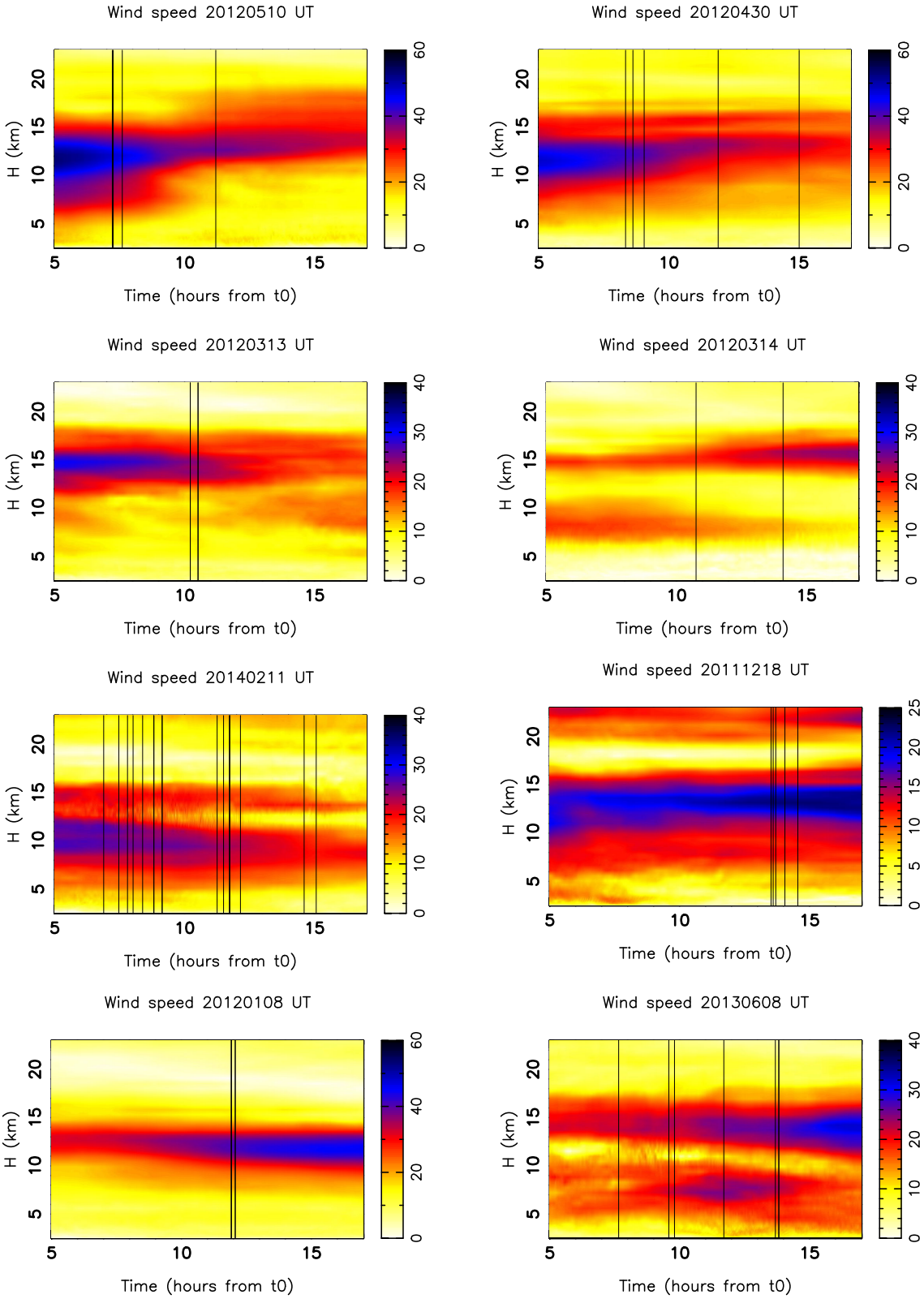

Figure 3. Temporal evolution of the WS for the whole atmosphere 20 km as recovered by the Meso-NH model during a few nights. The wind speed expressed in m s^{-1} is reported in the colour legend. Time is displayed on the x-axis, starting from 5 h after the beginning of the simulation (1900 LT). Simulations end 17 h after the beginning of the simulation (0700 LT). The figure therefore displays the night-time. Black vertical lines indicate the time at which measurements from GeMS are available. [A colour version of this figure is available in the online version.]

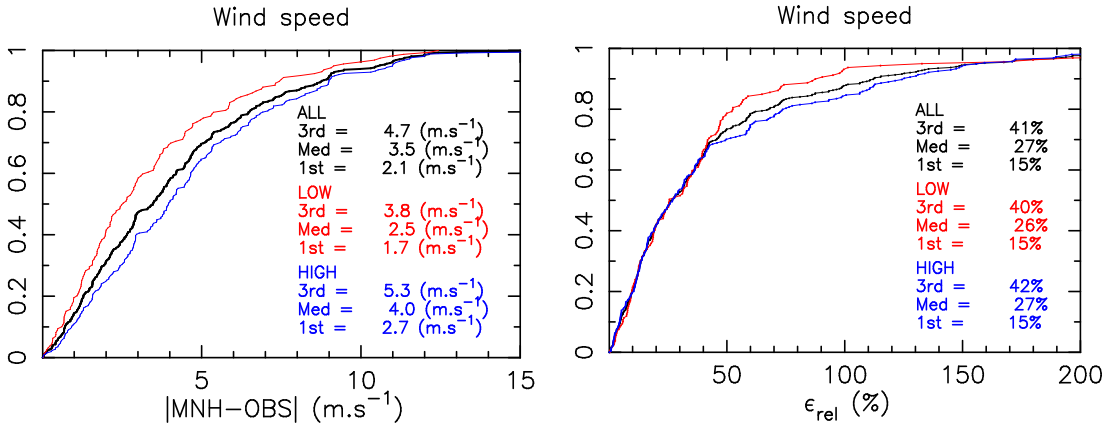

Figure 4. Left: cumulative distribution of the absolute difference of WS estimated by GeMS and by the model (400 points in the sample). The sample contains estimations referring to the [5 km, 18 km] a.s.l. range, i.e. the high part of the atmosphere (blue line), the [3 km, 5 km] a.s.l. range, i.e. the low part of the atmosphere (red line), and the [3 km, 18 km] a.s.l. range, i.e. the total atmosphere (black line). Right: cumulative distribution of the relative error of the WS in the same vertical slabs. There are no GeMS estimations for heights $h > 18$ km a.s.l. [A colour version of this figure is available in the online version.]

[observation, model output] estimates. Fig. 4 shows the cumulative distribution of the absolute difference of the WS quantified by the model and by GeMS (as in equation 1) with the associated error (as in equation 2) in three different vertical regions of the atmosphere – the high part of the atmosphere [5 km, 18 km], the low part of the atmosphere [3 km, 5 km] and the total atmosphere [3 km, 18 km]:

$$|V_{\mathrm{MNH}} - V_{\mathrm{OBS}}|\,, \tag{1}$$

$$\varepsilon_{\mathrm{rel}} = \frac{|V_{\mathrm{MNH}} - V_{\mathrm{OBS}}|}{V_{\mathrm{MNH}}} \times 100\,\text{per cent}. \tag{2}$$

There are no GeMS measurements of WS at heights greater than 18 km. All heights are above sea level (a.s.l.). We performed the comparison using the following procedure: (1) we take the measurements of GeMS $\pm$ the error bar along the z-axis; (2) the differences between model and GeMS estimates are calculated inside this vertical slab. Fig. 4 (right side) reports median values of 26, 27 and 27 per cent for relative errors in the low, high and total parts of the atmosphere, respectively. We obtained similar results by calculating the relative error with respect to the WS of GeMS instead of the WS of the model (this consists of replacing the respective values at the denominator in equation 2). The median value of the difference $|V_{\mathrm{OBS}} - V_{\mathrm{MNH}}|$ in the low, high and total atmosphere is 2.5, 4 and 3.5 m s^{-1} respectively, as shown in Fig. 4 (left side). We note that, at the first vertical grid point, model values are taken starting from 3 km a.s.l. (therefore 400 m above the ground) so as to use the model in more or less the same part of the atmosphere in which it has been validated by comparison with radiosoundings.[4] Between 30 and 400–500 m (what we called the *grey zone*), it is meaningless to compare Meso-NH and radiosounding estimates because of topographic effects (see Masciadri et al. 2013 for an extended discussion) and we can retrieve no conclusions. On the other hand, the model behaviour close to the surface (in the first 30 m above the ground) has been validated by comparing simulations with measurements provided by a meteorological station (Lascaux, Masciadri & Fini 2013, 2015). Those studies provided a very good correlation between the model and measurements made by sensors located at different heights. This guarantees that the model can be considered a good reference for the surface layer too. In this analysis, we observed that GeMS observations never fall in the grey zone. We conclude, therefore, that the model versus GeMS comparison is done in a consistent way in the region where the model has previously been validated (Masciadri et al. 2013).

The bias, RMSE and σ of the data set in the whole atmosphere, the high part [5 km, 18 km] a.s.l. and the low part [3 km, 5 km] a.s.l. is shown in Table 2. σ is the bias-corrected RMSE (equation 3):

$$\sigma = \sqrt{\mathrm{RMSE}^2 - \mathrm{BIAS}^2}. \tag{3}$$

In order to provide a more complete discussion of results, the corresponding values related to the comparison between the Meso-NH estimations and 50 radiosoundings (Masciadri et al. 2013) are reported in the same table. These last values refer to the study in which it was proven that Meso-NH is a reliable method for estimation of WS and WD, i.e. the study that lead us to consider Meso-NH as a reference in this study. It is possible to note that bias, RMSE and σ are in very good agreement between the Meso-NH model and GeMS. The statistical operators are only slightly larger than those estimated in the Masciadri et al. (2013) study. The difference for σ is of the order of 1.5 m s^{-1} in the low as well as the high part of the atmosphere. However, in this study we had to compare GeMS and model outputs within a larger Δh than considered in Masciadri et al. (2013); basically, a Δh corresponding to the different resolution of GeMS. It is, therefore, not surprising to obtain a slightly larger error. It does not mean that the results are worse. It simply indicates that we have to consider a larger uncertainty in the measurements due to the resolution, but the principle of detection works properly. Considering the strong shear of the wind at this height, we consider therefore that the agreement between Meso-NH and GeMS is very satisfactory.

Fig. 5 reports an example related to one night, during which a set of estimations of the wind speed as detected by GeMS at different instants of the night is shown (blue dots). In the same figure, the vertical WS profile as reconstructed by Meso-NH is reported for the same instants of GeMS observations. GeMS estimations are clearly in great agreement with estimations obtained with the Meso-NH model (black continuous line). Concerning the model estimates, we chose the profiles closest to the time at which

[4] In Masciadri et al. (2013), we considered 500 m instead of 400 m, because of a slight difference in the altitude of Cerro Paranal and Cerro Pachón. The definition of the grey zone is qualitative; therefore 500 or 400 m does not produce a great difference.

Table 2. Bias, RMSE and σ between the model and GeMS estimations calculated in low and high parts of the atmosphere using the whole sample of 43 nights. Bias is |MNH − OBS|.

	GeMS versus Meso-NH			Meso-NH versus radiosoundings[a]		
	43 nights			50 nights		
	m s^{-1}			m s^{-1}		
Vertical slab	bias	RMSE	σ	bias	RMSE	σ
LOW: [3,5] km a.s.l.	0.47	4.36	4.33	−1	3	2.83
HIGH: [5,18] km a.s.l.	−1.49	5.15	4.9	0.6	3.5	3.45

Note. [a]Referring to Masciadri et al. (2013).

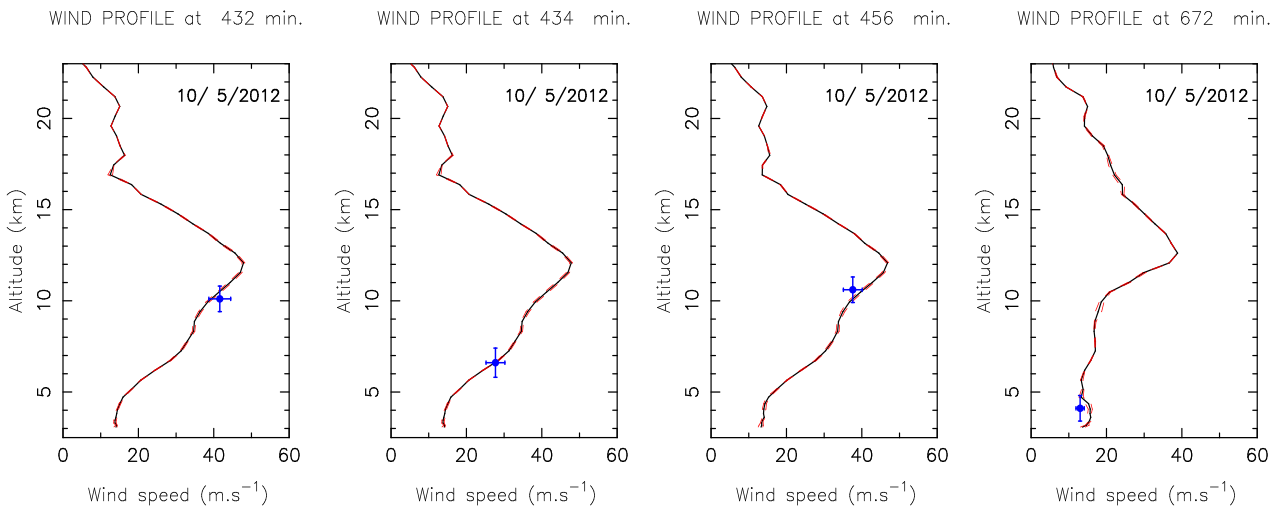

Figure 5. Example of WS as provided by GeMS (blue dots) and Meso-NH (vertical profile – black continuum line) during the same night. Red dashed lines are the maximum and minimum variation of the wind speed as simulated by the model in the temporal window ±8 min with respect to the closest GeMS measurement. See text for error bars on the x and y-axes. [A colour version of this figure is available in the online version.]

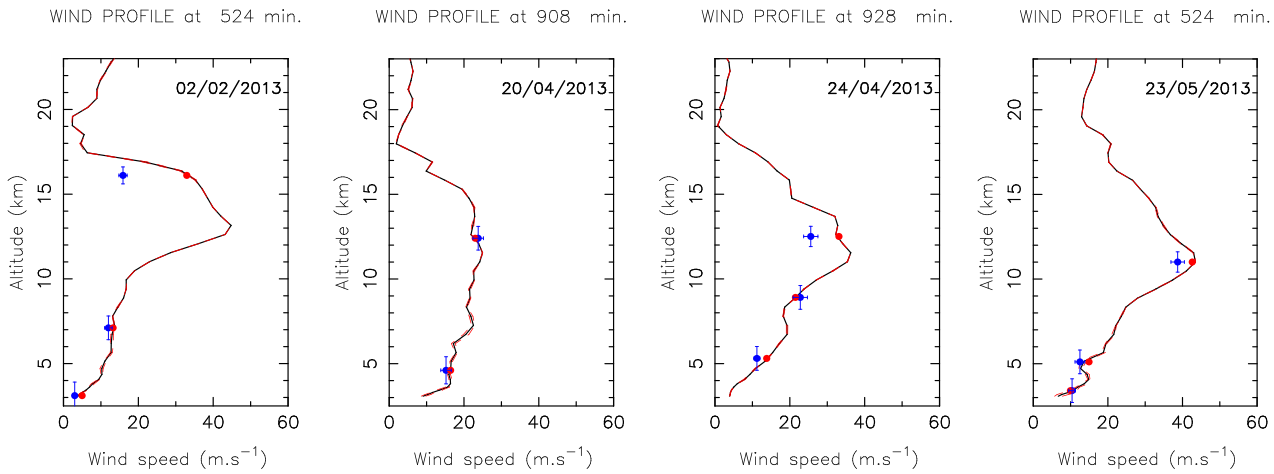

Figure 6. Examples of WS estimates as provided by GeMS (blue dots) and Meso-NH (vertical profile – black continuum line) during a few different nights. See Fig. 5 and the text for error bars on the x and y-axes. Nights during which GeMS detected the largest number of layers are shown. In general, no more than three layers for the WS have been detected by the system. The red dots are displayed on the vertical profile simply to indicate the same heights as the blue dots and facilitate the comparison from a visual point of view. [A colour version of this figure is available in the online version.]

observations have been made with respect to the temporal sampling of 2 min of Meso-NH (black continuum line). The maximum and minimum values calculated for a number of profiles selected at ±8 min with respect to the black line, i.e. ±4 profiles (dashed red lines), are also displayed. In Fig. 6, we show the wind speed as reconstructed by the model and as measured by GeMS for a number of nights during which GeMS identified the highest number of turbulent layers where it was possible to perform WS measurements (in the sample of 43 nights, a maximum number of three layers has been detected). For the total sample of 43 nights, we can state that the z-axis error bar (± error bar) of blue dots (GeMS measurements) is within the ±[0.5, 0.8] km range and the x-axis error bar is within the ±[0.5, 3.8] m s^{-1} range. Looking at Fig. 6, it is possible to note that, in most cases, the WS observed by GeMS and retrieved

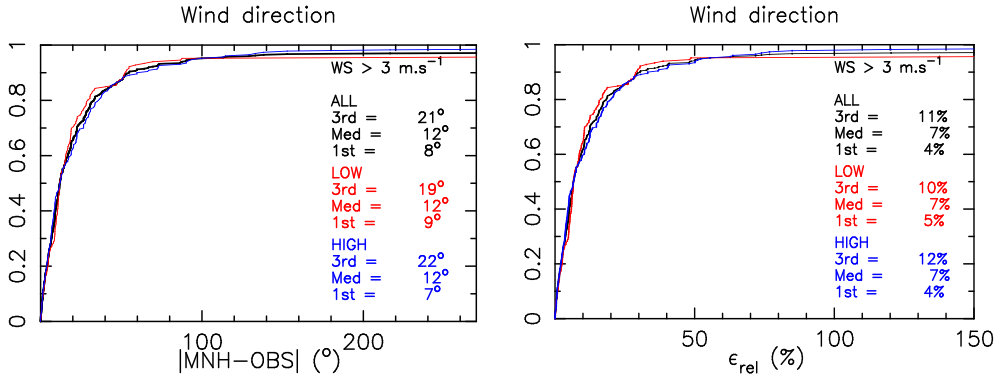

Figure 7. Left: cumulative distribution of the absolute difference of WD estimates retrieved by Meso-NH and GeMS (400 points in the sample). The sample contains estimations associated with the [5 km, 18 km] a.s.l. range, i.e. the high part of the atmosphere (blue line), the [3 km, 5 km] a.s.l. range, i.e. the low part of the atmosphere (red line), and the [3 km, 18 km] a.s.l. range, i.e. the total atmosphere (black line). Right: cumulative distribution of relative error in the same vertical slabs. There are no GeMS estimates for heights $h > 18$ km a.s.l. [A colour version of this figure is available in the online version.]

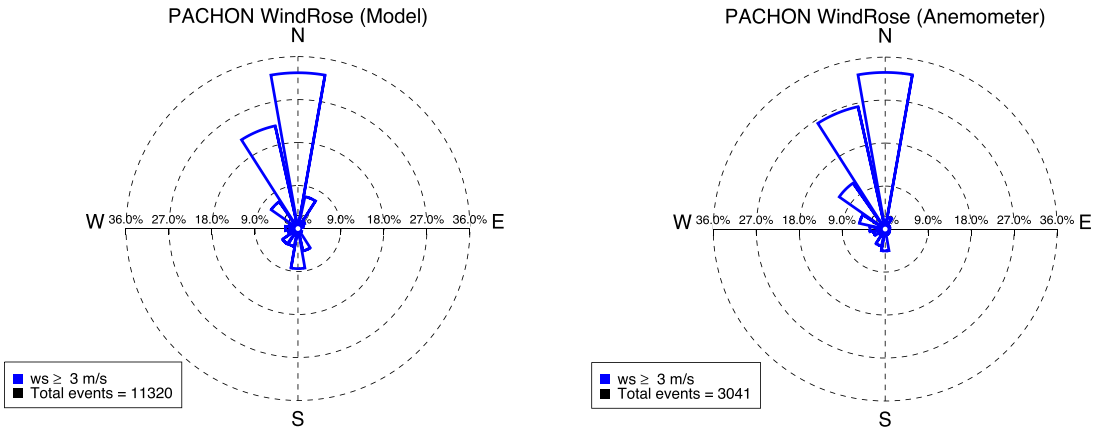

Figure 8. WD histogram retrieved by Meso-NH (left) and measured by the *in situ* anemometer (right) for the sample of 43 nights. Observations and simulations having a wind speed weaker than 3 m s^{-1} are filtered out.[A colour version of this figure is available in the online version.]

by Meso-NH is excellent. Only in one case (2013 February 2), at almost 16 km a.s.l., is the WS difference between GeMS and the model slightly larger. Of course, it is not possible to know which of the two (measurement or model estimate) is correct in this specific context. In general, the wind shear, particularly that associated with climatologic features besides the jet stream at these spatial scales, is very well reconstructed by this atmospheric model (see for example Masciadri et al. 2013, appendix B). Wind shear is associated with dynamic instabilities that are at the base of the hydrodynamic codes. Moreover, we note that the vertical resolution of the model is almost better than a factor of three with respect to SLODAR at this height. This is more in favour of a correct wind speed from the model. Also, we observe that, at this height, the wind speed shear is very important. This means that a very small underestimation by GeMS along z should be associated with a much better correlation with the model. In other words, the discrepancy should not be so important. Last but not least, we cannot exclude, even if it is less probable, the suggestion that it is the model that slightly overestimates the WS.

4.2 Wind direction

As for the wind speed case, we compared, for the same sample of 43 nights, measured and simulated wind directions for the whole 20 km above the ground. Fig. 7 reports the cumulative distribution of the absolute difference of WD as measured by GeMS and estimated by Meso-NH (as well as the relative error) using the same criteria used for the wind speed. We observe that the median values for both parameters are excellent, with values as small as 12° (7 per cent) in all the [3 km, 5 km] a.s.l., [5 km, 18 km] a.s.l. and [3 km, 18 km] a.s.l. ranges. We divided the atmosphere into these two ranges in order to have two samples that are statistically relevant. For the wind direction, not only the median value but also the first and third terciles remain within the excellent range: a maximum value of 22 per cent for the absolute difference and 12 per cent for the relative error.

Fig. 8 shows the wind rose of the wind speed close to the ground for the same sample of 43 nights. The figure reports a histogram of the distribution of wind direction. Observations are related to the WS and WD measured by the anemometer located *in situ* at [25–30] m above the ground at Cerro Pachón. Model estimates are related to all bins included in the same vertical range. In both observations and simulations, WD measurements related to WS weaker than 3 m s^{-1} have been filtered out. Indeed, when the WS is very weak it is meaningless to identify the WD with great accuracy, because the uncertainty in the measurement becomes important. As can be seen in Fig. 8, observed and simulated wind direction estimates are in very good agreement and this is an independent further element that proves the robustness of the reference used in this article, i.e. the Meso-NH model outputs. We remember that results obtained on

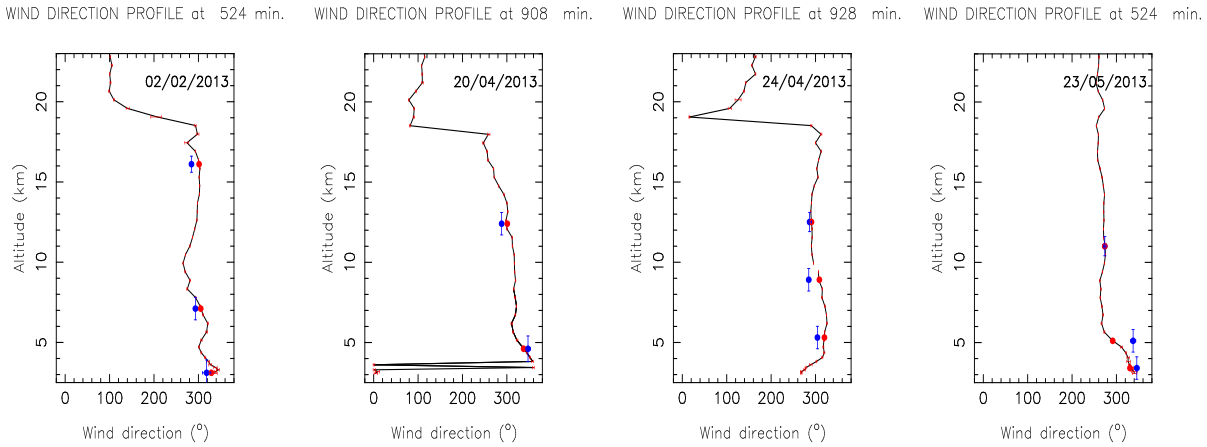

Figure 9. Examples of WD estimates as measured by GeMS (blue dots) and retrieved by Meso-NH (vertical profile – black continuous line) during different nights. Error bars with respect to the *y*-axis are the same as those of the wind speed case. Error bars along the abscissa are of the order of a few degrees and therefore not visible in the picture. The selected nights are the same as those related to Fig. 6. Typically GeMS identifies no more than three layers for the WS. The red dots are displayed on the vertical profile simply to indicate the same heights as the blue dots and facilitate the comparison. [A colour version of this figure is available in the online version.]

the occasion of the characterization of Cerro Pachón atmospheric conditions, from the perspective of the implementation of the Large Synoptic Survey Telescope (LSST: Els & Sebag 2011), indicate that the wind blows prevalently from the north-east and north-west in the surface layer above Pachón. We conclude that model estimates and measurements from anemometers, in relation to our sample of 43 nights, are in excellent agreement with the typical conditions above the Cerro Pachón site. All 400 measurements performed by GeMS are related to heights greater than 45 m a.g.l. and with a lower vertical resolution. It is therefore meaningless to consider the wind rose for the GeMS case.

Fig. 9 shows the wind direction at different heights as estimated by GeMS and retrieved by the model for the same set of nights analysed in Fig. 6. As already stated, these nights correspond to those with the largest number of estimates (typically three) at the same instant. Readers can observe how, in general, the variation of WD increases close to the surface and in the high part of the atmosphere (above the tropopause, i.e. above the jet-stream level). This is due to the fact that, in these regions, in general the wind speed decreases and the WD dispersion automatically increases. Looking at Fig. 9, it is possible to observe that, in basically all cases, the agreement of model versus GeMS is extremely good, as reflected by the statistical analysis shown in Fig. 7, giving a median value of the relative error of 7 per cent.

5 DISCUSSION

In previous sections, GeMS estimates have been compared with independent ones obtained with a non-hydrostatic numerical atmospheric model (Meso-NH) that was previously proved to be a robust estimator of WS and WD for the whole column of atmosphere [0–20] km. For this reason, it could be considered as a good reference. The agreement of such a comparison proved, in statistical terms, the validation of the SLODAR technique for wind estimates applied to MCAO systems. This is an important achievement (to our knowledge it the first time such a result has been published). However, we have to note that the automation of WS and WD measurement based on SLODAR techniques using a multiple set of sources is not trivial. The principle of detection implies, indeed, the identification of multiple cross-correlation peaks that are sometime not isolated. For routine and operational use of a MCAO (or more generally a WFAO) system, the SLODAR technique for WS and WD is, therefore, not very practical. Looking at Fig. 3, for example, the reader can deduce that, during each night, it is possible to isolate only a few estimates from GeMS. The temporal coverage is therefore extremely limited. Moreover, the automation of such a procedure is not trivial, mainly because such a system has been conceived to be an AO system and the measurement of atmospheric parameters has to be seen only as an ancillary output. This does sound like a criticism of the system, but is simply a realistic and pragmatic consideration. It should be much simpler, therefore, to feed WFAO systems directly with the Meso-NH WS and WD estimates. This solution implies the following advantages: (1) supplying information on WS and WD for a 20 km range above the ground, (2) doing this with a temporal sampling of ∼2 min (or even less) and (3) being available many hours in advance with respect to the observation. From a practical point of view, it should be much simpler to inject into GeMS the predictions of the model with the sequence of couples of (WS,WD) values all through the night some hours in advance, rather than recovering information on WS and WD from SLODAR technique estimates in real time. The AO system can therefore simply read the WS and WD value and use this information when it is required. Of course, this does not mean that it is meaningless to pursue studies of measurements performed with the SLODAR principle of cross-correlation on slopes coming from Shark–Hartmann systems of an MCAO system. However, the advantages related to use of the atmospheric model are scientific evidence.

Moreover, looking at Fig. 3, the important spatio-temporal variability of the wind speed over the whole 20 km, which might be different for each night, is clearly visible. This indicates that, in general, it should be suitable to know the WS and WD with a high frequency in time. The Meso-NH model can, in this sense, provide a more robust output with respect to measurements obtained from GeMS using the SLODAR technique. The high temporal frequency (2 min in this article) is definitely a very important added value. We note that the frequency of one measurement every two minutes, as provided by the model now, is sufficient to implement AO control. The fact that it might be, in principle, possible to use a higher frequency (shorter temporal interval) tells us that the

predictions provided by Meso-NH (WS and WD) might be useful in evaluating the validity of the assumption of 'frozen turbulence' in all those cases dealing with control techniques as described in the Introduction (Gavel & Wiberg 2002; Poyneer et al. 2007; Ammons et al. 2012; Ono et al. 2017). We do not exclude the suggestion that, under the assumption of a better signal-to-noise ratio of the MCAO system, measurements and model outputs might be used in a complementary way. This means, for example, that when the measurement performed with the MCAO system is missing, the model can replace the information. In any case, the goal of this article is not to propose a detailed solution but rather to guarantee that an automatic solution can be found because we have reliable model outputs.

GeMS is the first laser-assisted MCAO system running on the sky and this study proves, for the first time, that the SLODAR technique method for wind estimates with multiple sources provides reliable results, in agreement with an independent reference validated previously. Besides this, the development of other WFAO systems for 8–10 m class telescopes is in progress (among these, we recall the Adaptive Optics Facility (AOF) at the Very Large Telescope (Arsenault et al. 2014; Madec et al. 2016; Kuntschner et al. 2012) and Large Binocular Telescope INterferometric Camera – Near InfraRed and Visible Adaptive iNterferometer for Astronomy (LINC-Nirvana) at the Large Binocular Telescope (Herbst et al. 2016)); others will be implemented on the ELT class, such as the Multi-conjugated Adaptive Optics Relay (MAORY: Diolaiti et al. 2016), the AO system of the High Angular Resolution Monolitic Optical and Near-infrared Integral field spectrograph (HARMONI: Neichel et al. 2016; Thatte et al. 2016) and the Multi-Object Spectrograph (MOSAIC: Hammer et al. 2016; Morris et al. 2016) at the European Extremely Large Telescope (E-ELT), Narrow Field Infrared Adaptive Optics System (NFIRAOS) at the Thirty Metre Telescope (TMT: Boyer et al. 2014) and Giant Magellan telescope Adaptive Optics (GMTAO) at the Giant Magellan Telescope (GMT: Bouchez et al. 2014). Additionally, a few demonstrators for ELT WFAO systems have already seen the first sky time (CANARY (Gendron et al. 2016) at the William Hershel Telescope and RAVEN (Lardiere, Andresen & Blain 2014) at the SUBARU Telescope). This study might therefore be taken as a demonstrator for several operational AO and WFAO systems of the forthcoming generation of telescopes.

For completeness, we observe that some preliminary results of this study have been published in a couple of articles (Neichel et al. 2014b; Masciadri et al. 2016). In the first one, some preliminary WS comparisons on a very small number of nights were presented. In the second, we encountered serious problems in the comparison of measured and simulated WD estimates. Important discrepancies have been observed and the reason for such discrepancies was not clear, nor whether the problem could be linked to GeMS or the model. Recently, we identified the cause of such apparent problems. At that epoch, we were unaware of the existence of a flat mirror in the optical path of the GeMS, which flips the image plane of the wavefront sensor in the Y direction, making the Y component of the wind vector appear negative. The problem, which has now been corrected, was therefore neither in the model nor in GeMS, but in the way in which GeMS measurements were read. Moreover, in this article, new measurements (Gemini anemometer) permitted a precious independent confirmation of results related to WD. We are therefore in the condition of not only validating the GeMS instrument completely, but also proposing a strategy for an automatic WS and WD vertical profiler applied to WFAO systems.

6 CONCLUSIONS

In this article we prove, for the first time, the reliability of wind speed and direction measurements obtained with the MCAO system GeMS using a SLODAR technique and multiple laser guide star sources (Guesalaga et al. 2014). The reliability is proved by comparing GeMS estimates of the WS and WD with independent estimates of these parameters obtained with a non-hydrostatic atmospheric mesoscale model (Meso-NH). Such a model has been validated previously by comparing its estimates with 50 different radiosoundings (Masciadri et al. 2013, 2015). The level of agreement between the model and the radiosoundings was so good in statistical terms, as well as for each individual profile, that it definitely represents an excellent estimation for a cross-comparison with measurements in this study.

By performing the comparison (GeMS versus model) on a sample of 43 nights (corresponding to around 400 estimates), we find that both WS and WD estimates provided by GeMS are definitely reliable. The median value of the absolute difference of the GeMS and model WS is equal to 2.5, 4 and 3.5 m s^{-1}, respectively, in the [3 km, 5 km], [5 km, 18 km] and [3 km, 18 km] a.s.l. ranges, i.e. in the low, high and total atmosphere. Looking at the results in terms of relative errors, we find for the three ranges median values of 26, 27 and 27 per cent in the three regions. Results obtained for the WD are even better: we obtained, for all three regions, a median value of the absolute difference of the WD from GeMS and the model equal to 12° and a relative error equal to 7 per cent. The first and third terciles of WD are within 22 per cent.

For an operational application in an operational configuration, we propose, in this article, to inject the prediction of WS and WD coming from the Meso-NH model into GeMS. This solution is conceived as an alternative to the use of the SLODAR technique. It is, indeed, hard to transform the SLODAR method into an automatic procedure, due to its intrinsic limitations (see detailed discussion in Section 5). Among these, the main constraint is the difficulty in detecting isolated cross-correlation peaks that are, on the contrary, frequently overlapped. The method we propose presents several advantages (see details in Section 5). Besides this, the fact that both methods, i.e. the SLODAR techniques applied to a MCAO system and the mesoscale model Meso-NH, visibly provide coherent WS and WD estimates speaks in favour of the mutual reliability of the two methods. This is certainly useful, particularly for operational application, in which, as we discussed in Section 5, use of the WS and WD provided from the mesoscale model and GeMS can be complementary.

This study can be considered, therefore, as a demonstrator for the operational estimation of WS and WD along the 20 km of the atmosphere above the ground for any WFAO system.

Concerning the perspectives, it is worth saying that it is known that WFAO systems require not only knowledge of WS(h) and WD(h) to optimize their design and to run operationally, but also knowledge of the optical turbulence stratification (i.e. $C_N^2(h)$). As remembered in Section 2, the optical turbulence stratification can also be retrieved using measurements of slopes obtained by a SLODAR technique, with some small differences with respect to the calculation of the WS and WD. Starting from the original (Cortes et al. 2012) study, in recent years some diversification and improvements of the original method have been proposed (Ono et al. 2017; Guesalaga et al. 2017). C_N^2 vertical profiles can also be retrieved by the Astro-Meso-NH model (Masciadri et al. 2017), but for the optical turbulence it should not be realistic to use the model as a reference. In contrast, C_N^2 measurements provided by GeMS might

be used as a reference to investigate the ability of Astro-Meso-NH in predicting the optical turbulence above Cerro Pachón. This is the next step we envisage undertaking in the future.

ACKNOWLEDGEMENTS

Based on observations obtained at the Gemini Observatory, which is operated by the Association of Universities for Research in Astronomy, Inc., under a cooperative agreement with the NSF on behalf of the Gemini partnership: the National Science Foundation (United States), the National Research Council (Canada), CONICYT (Chile), Ministerio de Ciencia, Tecnología e Innovación Productiva (Argentina) and Ministério da Ciência, Tecnologia e Inovaçaõ (Brazil). Some of the Meso-NH simulations were run on the HPCF cluster of the European Centre for Medium Weather Forecasts (ECMWF) – Project SPITFOT. We acknowledge the Meso-NH Users's support team. AG thanks Conicyt-Chile, grant Fondecyt 1160236. This work has been partially funded by the ANR French program – WASABI.

REFERENCES

Ammons S. M., Potneer L., Gavel D. T., Kupke R., Max C. E., Johnson L., 2012, Proc. SPIE, 8447, 84471U
Arakawa A., Messinger F., 1976, GARP Tech. Rep. 17. WMO/ICSU, Geneva, Switzerland
Arsenault R. et al., 2014, The Messenger, 156, 2
Asselin R., 1972, Mon. Weather. Rev., 100, 487
Bouchez A. et al., 2014, Proc. SPIE 9148, 91480W
Bougeault P., Lacarrère P., 1989, Mon. Weather. Rev., 117, 1972
Boyer C. et al., 2014, Proc. SPIE, 9148, 91480X
Conan J. M., Le Roux B., Bello D., Fusco T., Rousset G., 2001, in Vernet E., Ragazzoni R., Esposito S., Hubin N., eds , ESO Conf. Workshop Proc., Vol. 58, Beyond Conventional Adaptive Optics. p.209
Cortés A., Neichel B., Guesalaga A., Osborn J., Rigaut F., Guzman D., 2012, MNRAS, 427, 2089
Costille A., Fusco T., 2012, Adaptive Optics Systems III, Proc. SPIE, 8447, 844757
Crampton D. et al., 2000, in Masanori I., Alan F. M., eds , Proc. SPIE Conf. Vol. 4008, Optical and IR Telescope Instrumentation and Detectors. SPIE, Bellingham, p.114
Cuxart J., Bougeault P., Redelsperger J.-L., 2000, Q. J. R. Meteorol. Soc., 126, 1
Diolaiti E. et al., 2016, Proc. SPIE, 9909, 99092D,
Ellerbroek B. L., 1994, J. Opt. Soc. Am. A, 11, 783
Els S. G., Sebag J., 2011, Revista Mexicana de Astrofisica Serie Conferencias, 41, 79
Elston R., Raines S. N., Hanna K. T., Hon D. B., Julian J., Horrobin M., Harmer C. F., Epps H. W., 2003, Proc. SPIE, 4841, 1611
Fusco T., Conan J. M., Michau V., Mugnier L., Rousset G., 1999, Optics Lett., 24, 1472
Fusco T., Conan J. M., Rousset G., Mugnier L., Micheau V., 2001, J. Opt. Soc. Am. A, 18, 2527
Gal-Chen T., Sommerville C. J., 1975, J. Comput. Phys., 17, 209
Garcia-Lorenzo B., Fuensalida J. J., 2011a, MNRAS, 410, 934
Garcia-Lorenzo B., Fuensalida J. J., 2011b, MNRAS, 416, 2123
Gavel D. T., Wiberg D., 2002, Proc. SPIE, 4839, 890
Gendron E. et al., 2016, Proc. SPIE 9909, Adaptive Optics Systems V, 99090C
Gilles L., Ellerbroek B. L., 2010, J. Opt. Soc. Am. A, 27, A76
Guesalaga A., Neichel B., Cortes A., Bechet C., Guzman D., 2014, MNRAS, 440, 1925
Guesalaga A., Neichel B., Correia C., Butterley T., Osborn J., Masciadri E., Fusco T., Sauvage J. F., 2017, MNRAS, 465, 1984
Hagelin S., Masciadri E., Lascaux F., 2010, MNRAS, 407, 2230
Hagelin S., Masciadri E., Lascaux F., 2011, MNRAS, 412, 2695
Hammer F. et al., 2016, Proc. SPIE, 9908, 990824,
Herbst T. et al., 2016, Proc. SPIE, 9908, 99080N
Hibon P. et al., 2014, Proc. SPIE, 9147, 91474U
Hibon P. et al., 2016, MNRAS, 461, 507
Johnson L. C., Gavel D. T., Reining M., Wiberg D. M., 2008, Proc. SPIE, 70153F
Johnston D. C., Welsh B. M., 1994, J. Opt. Soc. Am. A, 11, 394
Juvenal R., Kulcsár C., Raynaud H.-F., Conan J.-M., 2016, Proc. SPIE, 9909, 99090M,
Kuntschner H. et al., 2012, Proc. SPIE, 8448, Observatory Operations: Strategies, Processes, and Systems IV, 844808
Lafore J.-P. et al., 1998, Ann. Geophys., 16, 90
Lardiere O., Andresen D., Blain C., 2014, Proc. SPIE 9148, Adaptive Optics Systems IV, 91481G
Lascaux F., Masciadri E., Hagelin S., 2011, MNRAS, 411, 693
Lascaux F., Masciadri E., Fini L., 2013, MNRAS, 436, 3147
Lascaux F., Masciadri E., Fini L., 2015, MNRAS, 449, 1664
Le Louarn M., Tallon M., 2002, J. Opt. Soc. Am. A, 19, 912
Madec P. Y. et al., 2016, Proc. SPIE 9909, Adaptive Optics Systems V, 99090Z
Masciadri E., Egner S., 2006, PASP, 118, 1604
Masciadri E., Garfias T., 2001, A&A, 366, 708
Masciadri E., Vernin J., Bougeault P., 1999, A&AS, 137, 185
Masciadri E., Avila R., Sanchez L. J., 2004, Rev. Mex. Astron. Astrofis., 40, 3
Masciadri E., Lascaux F., Fini L., 2013, MNRAS, 436, 1968
Masciadri E., Lascaux F., Fini L., 2015, J. Physics: Conf. Ser., 595, 012020
Masciadri E., Neichel B., Guesalaga A., Turchi A., 2016, Proc. SPIE 9909, Adaptive Optics Systems V, 99093B
Masciadri E., Lascaux F., Fini L., 2017, MNRAS, 466, 520
Mc Gregor P. et al., 2004, Proc. SPIE, 5492, 1033
Morris T. et al., 2016, Proc. SPIE 9909, Adaptive Optics Systems V, 99091I
Neichel B., Fusco T., Conan J. M., 2008, J. Opt. Soc. Am. A, 26, 219
Neichel B. et al., 2014a, MNRAS, 440, 1002
Neichel B., Masciadri E., Guesalaga A., Lascaux F., Bechet C., 2014b, Proc. SPIE 9148, Adaptive Optics Systems IV, 914863
Neichel B. et al., 2016, Proc. SPIE 9909, Adaptive Optics Systems V, 990909
Noilhan J., Planton S., 1989, Mon. Weather. Rev., 117, 536
Ono Y. H., Akiyama M., Oya S., Lardiére O., Andersen D. R., Correia C., Jackson K., Bradley C., 2016, J. Opt. Soc. Am. A, 33, 726
Ono Y. H., Correia C. M., Anderson D. R., Lardiere O., Oya S., Akyyama M., Jackson K., Bradley C., 2017, MNRAS, 465, 4931
Osborn J., de Cos J., Guzman D., Butterley T., Myers R., Guesalaga A., Laine J., 2012, Optics Express, 20, 2420
Osborn J., Butterley T., Perera S., Fohring D., Wilson R., 2015, Adaptive Optics for Extremely Large Telescopes IV (AO4ELT4), Available at: http://escholarship.org/uc/ao4elt4, id. E52
Poyneer L., MacIntosh B. A., Veran J. P., 2007, J. Opt. Soc. Am. A, 24, 2645
Rigaut F. et al., 2014, MNRAS, 437, 2361
Sivo G. et al., 2013, in Esposito S., Fini L., eds, Proceedings of the Third AO4ELT Conference. Firenze, Italy, #127
Sivo G. et al., 2014, Optics Express, 22, 23565
Tallon M., Foy R., 1990, A&A, 235, 549
Thatte N. et al., 2016, Proc. SPIE 9909, Adaptive Optics Systems V, 99091X
Tokovinin A., Viard E., J. Opt. Soc. Am. A, 18, 873
Wang L., Schoek M., Chanan G., 2008, Appl. Optics, 47, 1880
Wilson R., 2002, MNRAS, 337, 103

This paper has been typeset from a TEX/LATEX file prepared by the author.